Citation: Molecular Therapy—Nucleic Acids (2014) 3, e160; doi:10.1038/mtna.2014.13

www.nature.com/mtna

RNAi-mediated Gene Silencing of Mutant Myotilin Improves Myopathy in LGMD1A Mice

Jian Liu[1], Lindsay M Wallace[1], Sara E Garwick-Coppens[1], Darcée D Sloboda[2], Carol S Davis[3], Chady H Hakim[4], Michael A Hauser[5,6], Susan V Brooks[2,3], Jerry R Mendell[1,7,8] and Scott Q Harper[1,7]

Recent progress suggests gene therapy may one day be an option for treating some forms of limb girdle muscular dystrophy (LGMD). Nevertheless, approaches targeting LGMD have so far focused on gene replacement strategies for recessive forms of the disease. In contrast, no attempts have been made to develop molecular therapies for any of the eight dominantly inherited forms of LGMD. Importantly, the emergence of RNA interference (RNAi) therapeutics in the last decade provided new tools to combat dominantly inherited LGMDs with molecular therapy. In this study, we describe the first RNAi-based, preclinical gene therapy approach for silencing a gene associated with dominant LGMD. To do this, we developed adeno-associated viral vectors (AAV6) carrying designed therapeutic microRNAs targeting mutant *myotilin* (MYOT), which is the underlying cause of LGMD type 1A (LGMD1A). Our best MYOT-targeted microRNA vector (called miMYOT) significantly reduced mutant myotilin mRNA and soluble protein expression in muscles of LGMD1A mice (the TgT57I model) both 3 and 9 months after delivery, demonstrating short- and long-term silencing effects. This MYOT gene silencing subsequently decreased deposition of MYOT-seeded intramuscular protein aggregates, which is the hallmark feature of LGMD1A. Histological improvements were accompanied by significant functional correction, as miMYOT-treated animals showed increased muscle weight and improved specific force in the gastrocnemius, which is one of the most severely affected muscles in TgT57I mice and patients with dominant *myotilin* mutations. These promising results in a preclinical model of LGMD1A support the further development of RNAi-based molecular therapy as a prospective treatment for LGMD1A. Furthermore, this study sets a foundation that may be refined and adapted to treat other dominant LGMD and related disorders.

Molecular Therapy—Nucleic Acids (2014) **3**, e160; doi:10.1038/mtna.2014.13; published online 29 April 2014
Subject Category: siRNAs, shRNAs, and miRNAs Therapeutic proof-of-concept

Introduction

Limb girdle muscular dystrophy (LGMD1A) is an autosomal dominant, adult-onset muscular dystrophy caused by mutations in the myotilin (*MYOT*) gene.[1,2] Disease progression in LGMD1A typically manifests first with weakness in the proximal muscles of the lower extremity, followed by proximal upper limb weakness. Eventually, distal leg and arm muscles become involved as well.[1–4] In addition to the limb muscle weakness that typifies all LGMDs, some patients with LGMD1A display unusual pharyngeal muscle involvement, causing dysarthric speech.[2,4] Nevertheless, presentation can vary among individuals with MYOT mutations.[1–9] Indeed, MYOT mutations have been identified as the most common underlying cause of myofibrillar myopathy (MFM; MFM3), which also affects limb muscles but has an inverse pattern of progression compared to LGMD1A.[7–9] Specifically, individuals with MFM typically develop distal limb muscle weakness first, with proximal involvement following later. MFM may also be associated with cardiac and respiratory muscle weakness and peripheral neuropathy. Interestingly, almost all LGMD1A- and MFM3-associated *MYOT* mutations are clustered to a region in exon 2 that encodes a serine-rich domain in the MYOT protein.[1–4,6–10] Thus, LGMD1A and MFM3 are genetically the same despite being classified as clinically distinct disorders, which has prompted the suggestion that the term "myotilinopathy" be used to reflect the allelism of these diseases.[4,7] For simplicity and to maintain consistency with previous publications, we have maintained the LGMD1A nomenclature when discussing the results in this manuscript.

The *MYOT* gene encodes a 57 kDa protein primarily expressed in skeletal muscle and bone marrow, with some weaker expression in heart.[2,11,12] Normal MYOT serves as a structural component of the Z-disc and is proposed to help organize the muscle cytoskeleton through various protein-protein interactions.[2,13–16] *MYOT* mutations cause the protein to misfold, lose solubility, and become increasingly resistant to turnover.[17] Combined, these factors lead to accumulation of mutant MYOT and its interacting proteins into intramuscular protein aggregates, which are a hallmark histopathological feature of LGMD1A and MFM.[4] Transgenic TgT57I mice, engineered to express skeletal muscle-specific MYOT containing a mutation found in humans with LGMD1A, develop muscular dystrophy and recapitulate LGMD1A-associated protein aggregates.[18] TgT57I aggregates become progressively larger and more abundant with time and likely impair

[1]Center for Gene Therapy, The Research Institute at Nationwide Children's Hospital, Columbus, Ohio, USA; [2]Department of Biomedical Engineering, University of Michigan School of Medicine, Ann Arbor, Michigan, USA; [3]Department of Molecular and Integrative Physiology, University of Michigan School of Medicine, Ann Arbor, Michigan, USA; [4]Department of Molecular Microbiology and Immunology, The University of Missouri, Columbia, Missouri, USA; [5]Department of Medicine, Duke University Medical Center, Durham, North Carolina, USA; [6]Department of Ophthalmology, Duke University Medical Center, Durham, North Carolina, USA; [7]Department of Pediatrics, College of Medicine, The Ohio State University, Columbus, Ohio, USA; [8]Department of Neurology, College of Medicine, The Ohio State University, Columbus, Ohio, USA. Correspondence: Scott Q Harper, Center for Gene Therapy, The Research Institute at Nationwide Children's Hospital, Columbus, 700 Children's Drive, Ohio 43205, USA. E-mail: scott.harper@nationwidechildrens.org
keywords: dominant muscular dystrophy; myotilin; myofibrillar myopathy; RNAi therapy; AAV; LGMD1A
Received 17 February 2014; accepted 21 March 2014; published online 29 April 2014. doi:10.1038/mtna.2014.13

function by physically disrupting the myofibrillar contractile apparatus, as well as by sequestering important MYOT-interacting structural proteins within the myofiber, including α-actinin, γ-filamin, desmin, and actin.[13–18] As MYOT-seeded protein aggregates accumulate with time, whole muscle specific force worsens in TgT57I mice.[18] Interestingly, TgT57I soleus and diaphragm muscles express soluble MYOT but lack aggregates, and show no significant differences from wild-type animals in force production.[18] Together, these data support that muscle contractile dysfunction in TgT57I mice is aggregation dependent.[18]

We hypothesized that treatments for LGMD1A should center on prevention or dissolution of MYOT-seeded protein aggregates. Accomplishing this requires reducing the load of mutant MYOT expression within affected muscle cells. To do this, we developed artificial miRNAs engineered to inhibit pathogenic MYOT expression in TgT57I LGMD1A mice.[19–21] In this report, we show that human *MYOT*-targeted miRNA shuttles reduce toxic MYOT aggregates and improve functional outcomes in TgT57I mice. This work represents an important first step toward demonstrating the potential for using RNA interference (RNAi)-based *MYOT* gene silencing approaches to treat LGMD1A and MFM3. In addition, it can be viewed as the initial plank in a broader program to develop therapeutic strategies for other dominant LGMD and MFM disorders using analogous RNAi-based therapies.[20–23]

Results

Identification of effective MYOT-targeting microRNAs

The first identified *MYOT* mutation was a C450T missense change resulting in a T57I amino acid conversion in the MYOT protein.[2] Transgenic mice engineered with muscle-specific expression of this mutant allele (T57I mice) recapitulate the progressive features of muscular dystrophy seen in human patients, including expression of the hallmark MYOT-positive protein aggregates and functional decline.[18] We hypothesized that *MYOT* knockdown, using an RNAi-based gene therapy, would improve LGMD1A-associated phenotypes in T57I mice. We therefore set out to develop artificial miRNA shuttle vectors based on human mir-30, in which mature mir-30 sequences were replaced with ones containing perfect antisense complementarity with the human *MYOT* mRNA.[21–24] We first designed four different U6 promoter-driven artificial microRNAs targeting human *MYOT*, which we referred to generally as miMYOTs, with individual sequences called mi1291, mi1321, mi1366, and mi1490 (**Supplementary Figure S1**). We then identified the most effective miMYOT using an *in vitro* gene silencing screen. Specifically, we transfected individual U6.miMYOTs or a U6.miGFP control[22,23] into HEK293 cells and measured *MYOT* mRNA and protein levels 48 hours later by real-time polymerase chain reaction (PCR) and western blot, respectively (**Figure 1a**). Sequence mi1321 consistently catalyzed the most robust knockdown against MYOT mRNA and protein levels in three different transfection experiments, with an average reduction of 81 and 62%, respectively (**Figure 1a**). The other three microRNAs (mi1291, mi1366, and mi1490) suppressed *MYOT* mRNA by 40, 58, and 45%, while protein levels were reduced only 16, 32, and 24% respectively, compared to the miGFP control. We therefore chose mi1321 as our lead microRNA for preclinical *in vivo* studies using T57I mice, and from this point forward refer to this sequence as miMYOT.

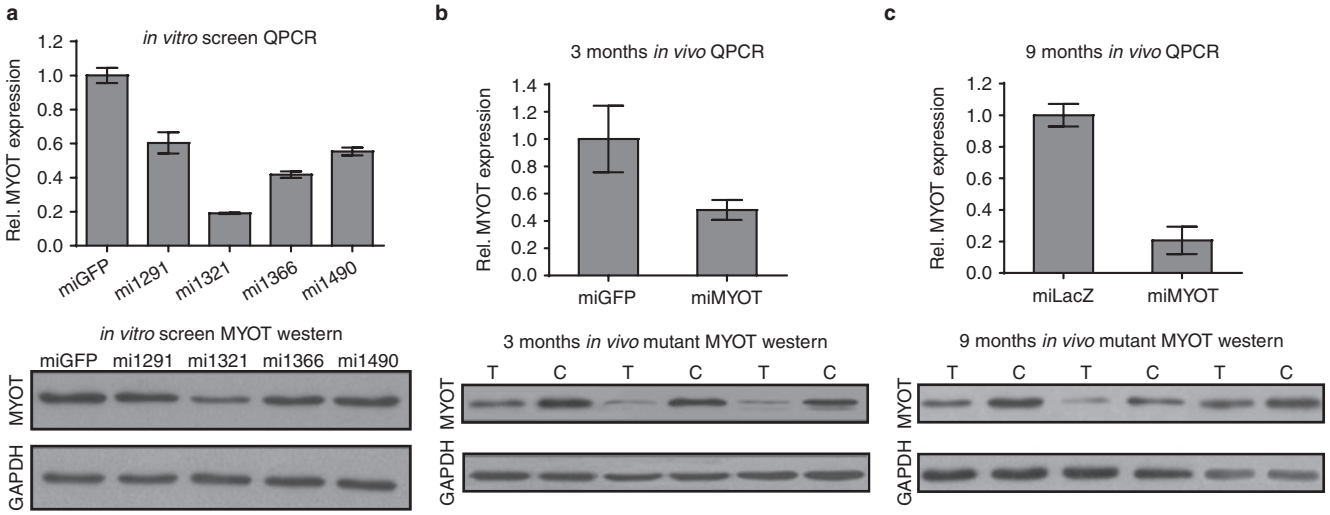

Figure 1 miMYOT mediates silencing of human myotilin *in vitro* and *in vivo*. (**a**) Four different MYOT-targeted artificial miRNAs (mi1291, mi1321, mi1366, and mi1490) were generated and tested for their ability to stimulate human *MYOT* gene silencing in HEK293 cells. Data shown are representative of three independent experiments. The lead miMYOT construct, mi1321, stimulated an 81 and 62% knockdown of *MYOT* mRNA (top, real-time PCR) and protein (bottom, western blot), respectively. Gene silencing data are calculated relative to samples transfected with a control miRNA targeting eGFP (miGFP).[22] Individual samples were normalized to GAPDH. The mi1321 construct is referred to as miMYOT in all subsequent figures. (**b**,**c**), AAV6-delivery of the U6.miMYOT construct to TgT57I mouse gastrocnemius muscle reduced mutant MYOT expression in 3- and 9-month-old animals, compared to AAV6-treated miGFP or miLacZ[29] controls, respectively. Specifically, by 3 months, MYOT mRNA and protein was reduced 50 and 54% and at 9 months, these values were 79 and 63%, respectively. For both timepoints, $N = 8$ animals, with one leg receiving AAV.miMYOT and the other a control miRNA vector. QPCR data represents means ± SEM. Western blots show three representative samples. C, control-treated legs; T, miMYOT-treated legs.

AAV6.miMYOT reduces MYOT expression in TgT57I mice *in vivo*

Adeno-associated viral vectors (AAV) are the current state-of-the-art delivery system for muscle gene therapy, with a proven safety profile in human clinical trials.[25–27] We have previous experience using AAV serotype 6 (AAV6) vectors for efficient muscle gene delivery, and employed this serotype again in this study.[22,23,28] To do this, we subcloned individual U6.miMYOTs or control sequences (targeting eGFP or LacZ) into a single-stranded AAV backbone coexpressing a GFP reporter from the CMV promoter and generated AAV6 particles.[22,23,29] We then injected 5×10^{10} DNAse-resistant particles of each vector into the lower limbs of newborn TgT57I or wild-type male littermates. Outcome measures were then performed at 3- and 9-month time points in the gastrocnemius muscle, which has significant disease involvement in human myotilinopathy patients and is among the most severely affected muscles in TgT57I mice. The two time intervals were chosen because TgT57I mice have well-developed myofibrillar aggregates and muscle weight deficits by 3 months of age and significant specific force deficits in the gastrocnemius muscle by 9 months.

We first examined AAV6 transduction efficiency by global GFP visualization in whole muscles (**Supplementary Figure S2**). As expected based on our previous work, AAV6.miMYOT and control vectors broadly transduced lower limb muscles of subject mice, both 3 and 9 months after injection (**Supplementary Figure S2**).[22,23] To confirm *MYOT* gene silencing *in vivo*, we measured transgenic mutant MYOT expression by real-time PCR and western blot. We found 50 and 54% average reductions of mutant human MYOT mRNA and protein, respectively, in 3-month-old T57I gastrocnemius muscles treated with AAV6.miMYOT compared to AAV6.miGFP controls injected in the contralateral leg (**Figure 1b**). Surprisingly, MYOT suppression was greater in 9-month animals, with 79 and 63% average reductions in human MYOT mRNA and protein, respectively (**Figure 1c**).

MYOT knockdown improves histopathology and muscle weight in 3-month-old TgT57I mice

TgT57I mice recapitulate the progressive MYOT protein aggregation defects that characterize LGMD1A. In 3-month-old TgT57I mice, aggregates are associated with additional generalized muscle pathology, including deficits in myofiber size and gastrocnemius muscle weight, as well as slight but significant increase in myofibers with centrally located nuclei, which is a histological indicator that muscles underwent degeneration and were subsequently repaired. Importantly, these phenotypes are useful outcome measures for RNAi therapy. We therefore examined the effects of miMYOT-mediated *MYOT* gene silencing on aggregate formation, myofiber diameter, muscle weight, and central nuclei defects associated with LGMD1A in young adult TgT57I mice.

We first examined aggregate accumulation by staining AAV6.miMYOT- and AAV6.control-treated TgT57I gastrocnemius muscle cryosections with MYOT immunoreactive antibodies, hematoxylin and eosin (H&E), and trichrome (**Figure 2a**,**b**). Microscopic image analysis showed that *MYOT* knockdown significantly reduced the abundance of protein aggregates by 69% in 3-month-old TgT57I gastrocnemius muscles (**Figure 2b**,**c**).

We next determined the impacts of *MYOT* inhibition on cross-sectional myofiber size using H&E stained muscle cryosections. As expected, myofibers from AAV.control-treated TgT57I muscles were significantly smaller (49.9 µm average diameter; $P < 0.05$) than those from either wild-type group (57.0 and 57.7 µm in wild-type mice receiving miMYOT or miGFP, respectively; **Figure 2d**). In contrast, *MYOT* knockdown by our therapeutic AAV6.miMYOT vector improved average myofiber diameter in TgT57I mice by 4.9 µm (a 9.8% improvement), to levels not significantly different than wild-type (54.8 µm in AAV6.miMYOT-treated TgT57I mice; **Fig 2d** and **Supplementary Figure S3**). This improvement in myofiber size defects evident at the cellular level translated to whole muscle as well. Indeed, weights of AAV6.miMYOT-treated TgT57I gastrocnemius muscles were not significantly different than those measured in wild-type–treated controls, while TgT57I muscles that received control AAV6.miGFP vector weighed an average of 15.9 mg less (11% decrease) than their wild-type counterparts ($P < 0.001$; **Figure 2e**). Finally, comparing the AAV6.miMYOT- and AAV6.miGFP-treated TgT57I animals, we found that *MYOT* knockdown improved 3-month TgT57I gastrocnemius muscle weight by an average of 9.5 mg, representing a significant 7.1% improvement ($P < 0.001$).

As a final measure of the effects of *MYOT* knockdown on LGMD1A-associated histopathology in 3-month-old TgT57I mice, we quantified the percentage of myofibers containing centrally located nuclei. Typically, ~98–99% of myonuclei in uninjured wild-type mouse muscles are localized to the cell periphery.[30] Consistent with this, gastrocnemius muscles from our AAV6.miMYOT- and AAV6.miGFP-treated wild-type animals showed 1.1 and 1.9% central nuclei, respectively (**Figure 2f** and **Supplementary Figure S3**). In contrast, 7.7% of 3-month TgT57I myofibers from control AAV6.miGFP-treated gastrocnemius muscles contained central nuclei. This value is consistent with mild degeneration and regeneration in dystrophic animals. Importantly, MYOT knockdown by AAV6.miMYOT reduced the percentage of myofibers with central nuclei to 3.6% in TgT57I mice, representing a significant 53% decrease ($P < 0.001$; **Figure 2f**; **Supplementary Figure S3**).

MYOT knockdown improves histopathology, muscle weight, and specific force in 9-month-old TgT57I mice

Gastrocnemius is among the most severely affected muscles in TgT57I mice and often in patients with *MYOT* mutations.[4,31,32] Although 3-month-old TgT57I muscles display LGMD1A-associated changes in histology and weight (**Figure 2**), our pilot studies showed that significant muscle weakness did not manifest until later in adulthood (9 months of age; **Supplementary Figure S4** and data not shown). This delayed functional decline in mice was consistent with the adult-onset nature of LGMD1A in humans. We reasoned that the 9-month mouse gastrocnemius muscle represented an excellent, though challenging, model of severe LGMD1A. We therefore treated a second cohort of animals with AAV6.miMYOT or control AAV6.miLacZ vectors for 9 months, with

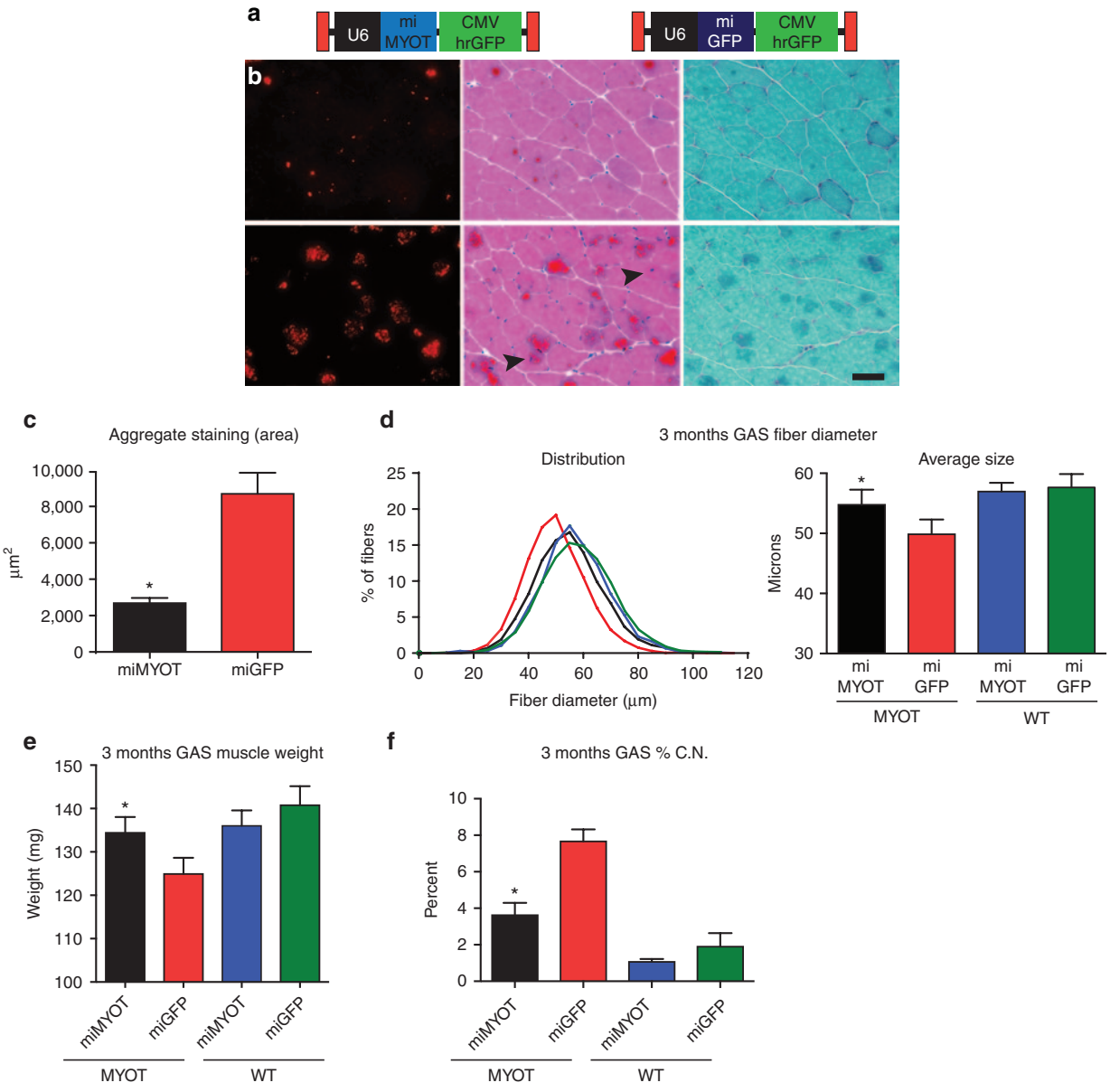

Figure 2 AAV.miMYOT improves histopathology and muscle weight in 3-month-old TgT57I mice. (**a**) AAV vectors used in 3-month studies. The miMYOT and control miGFP RNAs are expressed from the mouse U6 promoter. Both vectors contain a CMV.hrGFP reporter gene cassette. Red rectangles indicated adeno-associated virus (AAV)-inverted terminal repeats (ITRs). (**b**) Representative serial sections from TgT57I mice injected with AAV.miMYOT (top panels) or AAV.miGFP (bottom panels) controls show reductions in MYOT-seeded protein aggregates. Red spots are protein aggregates stained by immunofluorescence with MYOT antibodies. Middle panels show overlay with H&E-stained serial sections. Arrows indicate fibers containing centrally located myonuclei. Right panels, aggregates are visible as dark blue spots within the myofiber in serial sections stained with Gomori's Trichrome, while nuclei are purple. Scale bar, 50 μm. Images shown are representative of eight independently injected animals per virus. (**c**) Quantification of aggregate staining 3 months after injecting TgT57I gastrocnemius muscles with AAV.miMYOT or AAV.miGFP. MYOT knockdown significantly reduced the average area of MYOT-positive aggregates by 69% ($N = 5$ muscles per group; five randomly sampled fields per muscle; paired t-test, $P = 0.0069$; errors bars represent SEM). (**d**) Graphs show the distribution and average size of TgT57I and wild-type (WT) muscles treated with AAV.miMYOT or AAV.miGFP controls, 3 months postinjection. MYOT knockdown in TgT57I muscles significantly improved myofiber diameter by 4.9 microns (54.8 versus 49.9 μm in control-treated TgT57I mice; t-test, $P = 0.047$). WT fiber diameters were 57 and 57.7 microns, in miMYOT- and miGFP-treated animals, respectively. $N = 5$ muscles per group; five randomly selected fields per muscle; an average of 1,205 fibers counted per wild-type animal and 1,433 fibers per TgT57I animal). (**e**) AAV.miMYOT significantly improved GAS muscle weight by 9.5 mg in 3-month-old TgT57I mice (paired t-test, $P < 0.001$; $N = 12$ muscles per group). AAV.miMYOT-treated muscles averaged 134.4 mg in weight versus 124.9 mg in AAV.miGFP-treated animals; WT controls: miMYOT, 136.0 mg; miGFP, 140.8 mg). (**f**) The mild degeneration-regeneration effects in TgT57I muscles, as indicated by the presence of myofibers with centrally located nuclei, were significantly improved 2.1-fold with AAV.miMYOT treatment compared to controls (t-test, $P = 0.0004$). Both groups of TgT57I mice were still significantly different from respective WT controls (t-test, $P < 0.006$). For central nuclei counts, an average of 1,212 fibers were counted per wild-type animal and 1,498 per MYOT animal. *, indicates significant difference between miMYOT- and miGFP-treated TgT57I animals. Wild-type animals were not significantly different from one another by all measures, regardless of treatment.

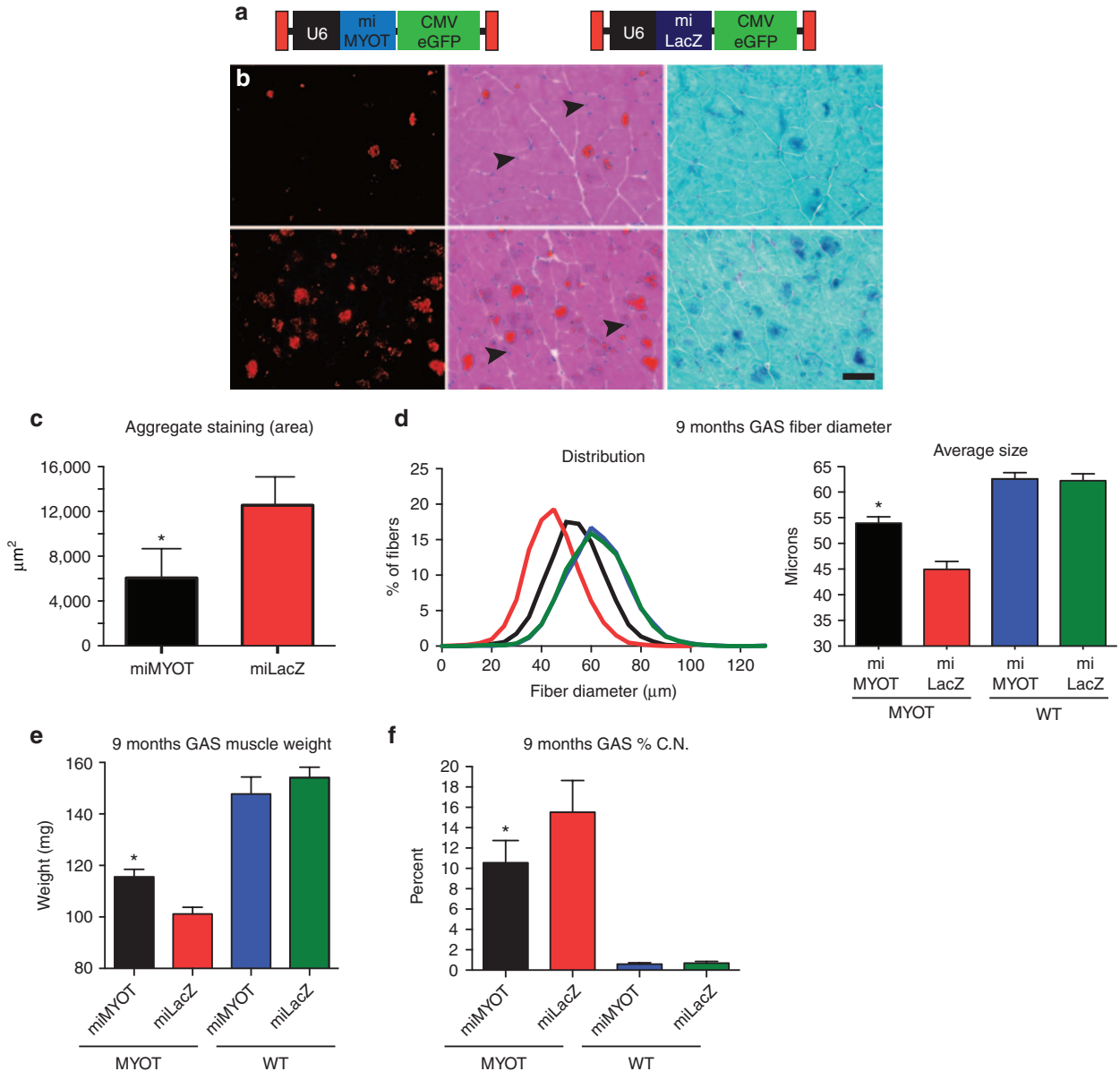

Figure 3 AAV.miMYOT improves histopathology and muscle weight in 9-month-old TgT57I mice. (**a**) AAV vectors used in 9-month studies. The miMYOT and control miLacZ RNAs are expressed from the mouse U6 promoter. Both vectors contain a CMV.eGFP reporter gene cassette. Red rectangles indicated AAV inverted terminal repeats (ITRs). (**b**) Representative serial sections from TgT57I mice injected with AAV.miMYOT (top panels) or AAV.miLacZ (bottom panels) controls show reductions in MYOT-seeded protein aggregates. Red staining represents protein aggregates labeled by immunofluorescence with MYOT antibodies. Middle panels show overlay with H&E-stained serial sections. Arrows indicate fibers containing centrally located myonuclei. Right panels, aggregates are visible as dark blue structures within the myofiber in serial sections stained with Gomori's Trichrome, while nuclei are purple. Scale bar, 50 µm. Images shown are representative of 8 independently injected animals per virus. (**c**) Quantification of aggregate staining 9 months after injecting TgT57I GAS muscles with AAV.miMYOT or AAV.miLacZ. MYOT knockdown significantly reduced the average area of MYOT-positive aggregates by 52% ($N = 5$ muscles per group; five randomly sampled fields per muscle; paired *t*-test, $P = 0.0085$; errors bars represent SEM). (**d**) Graphs show the distribution and average size of TgT57I and wild-type (WT) muscles treated with AAV.miMYOT or AAV.miLacZ controls, 9 months post-injection. MYOT knockdown in TgT57I muscles significantly improved myofiber diameter by 9.1 microns (54 versus 44.9 µm in control-treated TgT57I mice; *t*-test, $P = 0.0006$). WT fiber diameters were 62.5 and 62.2 microns, in miMYOT- and miLacZ-treated animals, respectively. These values were significantly larger than either TgT57I group ($P < 0.001$, *t*-test). $N = 5$ muscles per group; five randomly selected fields per muscle; an average of 993 fibers counted per wild-type animal and 1,554 fibers per TgT57I animal). (**e**) AAV.miMYOT significantly improved GAS muscle weight by 15 mg in 9-month-old TgT57I mice (paired *t*-test, $P = 0.002$; $N = 8$ muscles per group). AAV.miMYOT-treated muscles averaged 116 mg in weight versus 101 mg in AAV.miLacZ-treated animals; WT controls: miMYOT, 148 mg; miGFP, 154 mg). (**f**) The mild degeneration-regeneration effects in TgT57I muscles, as indicated by the presence of myofibers with centrally located nuclei, were significantly improved 2.1-fold with AAV.miMYOT treatment compared to controls (*t*-test, $P = 0.0004$). Both group of TgT57I mice were still significantly different from respective WT controls (*t*-test, $P < 0.0001$). For central nuclei counts, an average of 998 fibers were counted per wild-type animal, and 1,553 per MYOT animal. *, indicates significant difference between miMYOT- and miLacZ-treated TgT57I mice. Wild-type animals were not significantly different from one another by all measures, regardless of treatment.

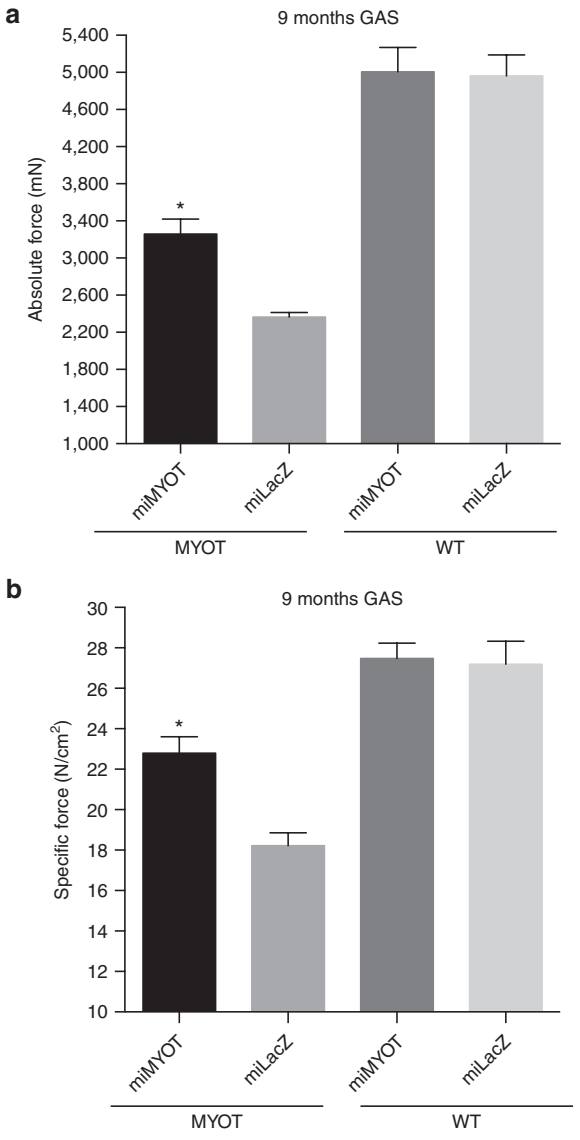

Figure 4 AAV.miMYOT significantly improves whole muscle strength in TgT57I mice 9 months after treatment. AAV.miMYOT-treated TgT57I GAS muscles showed statistically significant 38 and 25% improvements in (**a**) absolute force and (**b**) specific force compared to AAV.miLacZ-treated controls ($N = 6–8$ legs; $P = 0.0031$ for (**a**) and $P = 0.0009$ for (**b**), paired *t*-test). Both TgT57I groups were significantly weaker than their WT counterparts ($P < 0.0001$, *t*-test), while wild-type groups were not significantly different from one another.

the goal of correcting whole muscle functional deficits in aged TgT57I gastrocnemius muscles.

Before measuring specific force, we confirmed that MYOT suppression by AAV6.miMYOT (79% mRNA; 63% protein; **Figure 1c**) was still benefitting TgT57I animals at 9 months of age, using the outcome measures established in our younger, 3-month cohort. We found that AAV6.miMYOT-treated TgT57I animals showed significant correction by all measures, compared to AAV6.miLacZ control-treated counterparts. Specifically, in 9-month-old AAV6.miMYOT-treated TgT57I animals, aggregates were reduced by 52% ($P < 0.01$); myofibers were 9.1 µm (20%) larger (54 µm average in AAV.miMYOT-treated versus 44.9 µm average in AAV6.miLacZ-treated TgT57I; $P = 0.0006$); gastrocnemius muscles weighed 12% more (116 mg average in AAV.miMYOT-treated versus 101 mg average in AAV6.miLacZ-treated TgT57I; $P = 0.002$); and central nuclei were reduced 32% (10.6% in AAV6.miMYOT-treated versus 15.5% in AAV6.miLacZ-treated TgT57I; $P < 0.04$). We noted that the improvements afforded by AAV6.miMYOT were partial, as TgT57I animals treated with this therapeutic vector were still significantly different from wild-type groups using all outcome measures at 9 months (**Figure 3**).

Table 1 Summary of phenotypes in miMYOT- and control-treated TgT57I mice

	% Correction		Correction compared to WT	
Phenotype	3 months	9 months	3 months	9 months
MYOT expression				
mRNA	50% decrease	79% decrease	NA	NA
Soluble protein	54% decrease	63% decrease	NA	NA
Protein aggregates	69% decrease	52% decrease	NA	NA
GAS muscle parameters				
Myofiber diameter	9.8% increase	20% increase	No Δ from WT	Partial
Central nuclei	53% decrease	32% decrease	Partial	Partial
Muscle weight	7.1% increase	12% increase	No Δ from WT	Partial
GAS strength				
Absolute force	ND	38% increase	ND	Partial
Specific force	ND	25% increase	ND	Partial

GAS, gastrocnemius muscle; NA, not applicable; ND, not determined; WT, wild-type animals; Δ, change.

Importantly, we found that MYOT knockdown by AAV6.miMYOT caused significant functional improvement in TgT57I gastrocnemius muscles, as determined by whole muscle physiology tests. Specifically, we found that MYOT knockdown improved absolute and specific force in 9-month TgT57I gastrocnemius muscles by 38 and 25%, respectively (**Figure 4**). As with the other outcome measures described above, this represented a partial functional recovery, as both groups of TgT57I animals were significantly different from their wild-type–treated counterparts (**Figure 4**). All data for both time points are summarized in **Table 1**.

Discussion

Several years ago, our group began exploring the hypothesis that RNAi therapy could be useful for combating dominant muscle diseases. With this goal in mind, we have been working to show preclinical feasibility for this strategy, targeting two different dominant muscular dystrophies.[20–23] Initially, we focused on reducing expression of the *FRG1* and *DUX4* genes associated with facioscapulohumeral muscular dystrophy in mice.[20–23] We followed up in this study by showing that mutant *MYOT* inhibition by RNAi could improve abnormalities in the TgT57I mouse model of LGMD1A. Taken together, these data provided three preclinical examples to support

that RNAi might be broadly applied to treat a number of dominant muscle disorders, including facioscapulohumeral muscular dystrophy, LGMD1A, and possibly other forms of dominant LGMD and MFM.

We found that our RNAi treatment significantly improved several phenotypes associated with LGMD1A in both young (3 months) and old (9 months) TgT57I mice (**Figures 1–4**; summarized in **Table 1**). Of the outcome measures used, we observed the best miMYOT-mediated correction in gastrocnemius muscle weight and myofiber diameter from 3-month-old TgT57I mice. Indeed, miMYOT-treated TgT57I mice were not significantly different from wild-type counterparts using these metrics. For all other outcome measures (3- and 9-month central nuclei; 9-month myofiber diameter, gastrocnemius weight, and force parameters), correction was statistically significant but did not reach the same levels measured in wild-type animals (**Table 1**). Taken alone, this partial correction was encouraging because it suggested that RNAi therapy worked to alleviate abnormalities associated with LGMD1A in mice. However, the level of correction we achieved was even more impressive considering we targeted the most severely affected muscle in LGMD1A mice, and moreover, because these transgenic animals express 2.6-fold more mutant MYOT than wild-type protein (which is produced from its two intact normal MYOT alleles).[18]

Despite our promising results in a challenging model of LGMD1A, we did not completely restore all outcome measures to wild-type levels, and there is room for improvement. For example, our RNAi treatments reduced protein aggregate load from roughly ~15% to ~7% of total cross-sectional area in 9-month TgT57I gastrocnemius muscles, with accompanying partial improvements in muscle histology and function. This leads to the question: "Is complete resolution of protein aggregates required or can muscles tolerate some level of aggregate load and still function normally?" We hypothesize that complete resolution is not required to reach wild-type levels of correction, based on the progressiveness of the disease in humans and mice.[4,18] Indeed, humans express *MYOT* throughout their lives, but LGMD1A patients typically do not show overt functional deficits until late adulthood.[4,33] Likewise, aggregates appear in TgT57I mice by 2 weeks of age, but the animals do not develop significant histological deficits until 3 months of age, and functional abnormalities appear several months later.[18] Thus, there appears to be a tolerable threshold of aggregate expression in TgT57I mice below which muscles can function like those in wild-type animals. Before we think about translating this strategy further, it will be important to determine what this tolerance threshold is and if it can be reached using RNAi therapy in severely affected TgT57I mouse muscles.

One potential strategy to further reduce toxic *MYOT* expression is to increase the miMYOT dose delivered to TgT57I mice. In this initial study, we were limited by the amount of AAV6 that could be administered because we found that the *hrGFP* reporter gene in our first-generation vectors caused muscle toxicity when administered above $3–5\times10^{10}$ total particles.[34] We later switched to a less toxic *eGFP* vector (for 9-month studies) but delivered the same amount of vector to maintain consistency and because eGFP was also somewhat toxic to muscle at higher doses.[34] We note that switching the reporter gene from *hrGFP* to *eGFP* necessitated changing our control miRNA from miGFP (which targets *eGFP*) to miLacZ (which targets the *Escherichia coli LacZ* gene).[29] Importantly, both miRNAs were benign in mouse skeletal muscle. Nevertheless, future translational studies will require a new, next-generation vector that lacks a reporter gene and only expresses the therapeutic noncoding miMYOT RNA. Eliminating the reporter will help alleviate potential toxicity problems arising from expressing eGFP (or any foreign protein). In addition, it frees up space within the AAV genome, thereby more comfortably permitting packaging of the miMYOT expression cassette into a double-stranded, self-complementary AAV backbone, which transduces muscle 10–15 times better than single-stranded counterparts.[35] Thus, administering similar titers of self-complementary AAV.miMYOT could yield a 10- to 15-fold increase in miMYOT expression, while administering more vector particles (*e.g.*, to the $1–5\times10^{11}$ range) would further multiply the miMYOT dose to 50–150-fold above that achieved in this study. This may be an important consideration for future studies that could involve vascular delivery, which requires significantly more vector than intramuscular injection.[36,37]

Like any drug, inhibitory RNAs can be toxic when expressed at high levels, and it will therefore be important to monitor potentially adverse phenotypes in any dose-escalation study. We were encouraged that our preclinical data here already support the safety of our first-generation miMYOT sequences at moderate doses, since we did not note any deleterious effects from miMYOT expression in wild-type animals (**Figures 2–4**, **Supplementary Figures 3** and **4**). Moreover, preliminary toxicology studies of our miMYOT and miLacZ control vectors (which included CMV.eGFP) revealed no significant morbidity due to treatment in any animals (**Supplementary Figure S5**). Considering that we are using well-established AAV vector and delivery platforms with proven safety profiles in clinical studies, and our next-generation vectors, discussed above, will not express a protein-coding gene from the AAV genome, we are hopeful that the barriers to translating RNAi-based gene therapy will be lower than those encountered in recent history for gene replacement therapies of neuromuscular diseases.[38]

A final consideration regarding the design of the next generation of miMYOT vectors relates to the microRNA sequence. Although miMYOT (mi1321) proved safe and effective at moderate dosages in mice, additional MYOT-targeted microRNAs may be required in the next generation of vectors. The rationale for this is partly related to confirming our initial mi1321 results with an independent miMYOT sequence, and having more than one potential therapeutic option for future translational studies. However, another more complicated issue that may impact miMYOT design has to do with the requirement for normal *MYOT* in mice and humans. Specifically, mice do not require MYOT for normal development or muscle function; *MYOT* null mice are indistinguishable from wild-type animals, and show no evidence of muscular dystrophy or Z-disc malformations.[39] The lack of necessity for *MYOT* in mice meant that complicated disease allele-specific silencing strategies were not required to demonstrate proof-of-principle for this strategy. Thus, although miMYOT contained only one mismatched nucleotide with wild-type mouse *MYOT* and could theoretically reduce its

expression (**Supplementary Figure S1c**), we did not investigate normal *MYOT* expression levels in this study because they had no functional consequences. Unfortunately, it is not known if *MYOT* is required for normal human muscle development or homeostasis, since homozygous *MYOT* mutations have never been reported in humans with recessive myopathy. Certainly, this could suggest that *MYOT* absence is incompatible with normal human development, but the high level of conservation between the mouse and human genes (each with 10 exons encoding full-length 57 kDa proteins sharing 89% identity and 95% similarity at the amino acid level) suggests the opposite: *MYOT* absence is well tolerated in humans, and people with null alleles have not been identified because their muscles are normal. Nevertheless, it is puzzling why this highly conserved gene would also be nonessential. It has been suggested that MYOT absence is compensated for by upregulation of other structurally related proteins such as palladin and/or myopalladin.[39] Regardless, the uncertainty about the impacts of normal MYOT haploinsufficiency in humans suggests it may be prudent to design new miRNAs that selectively reduce expression of the mutant *MYOT* transcript while leaving the normal allele unperturbed.[40]

A final important question that needs addressing relates to the timing of inhibitory RNA administration. In this study, we delivered our AAV vectors to newborn LGMD1A mice prior to onset of obvious muscle abnormalities. These animals showed partial correction by 9 months of age, suggesting that our treatments served to slow disease onset and/or progression. This may be beneficial if this strategy was translated to humans, since LGMD1A is adult-onset and can take ~10 years to fully disable.[4] Nevertheless, ideally this strategy would inhibit *MYOT* gene expression enough to allow cellular protein degradation machinery to dissolve pre-existing aggregates and reverse-associated pathologies. Currently, we do not know if LGMD1A-associated protein aggregation is reversible, but prior studies in other similar disease models suggest the possibility. For example, like LGMD1A, Huntington's disease (HD) is a progressive disorder in which protein aggregates accumulate in postmitotic cells (primarily neurons in HD). In a seminal study, mice engineered to inducibly express a toxic HD transgene (called HD94) recapitulated intraneuronal protein inclusions and developed HD-like progressive neurodegeneration.[41] Importantly, 4 months after the HD94 transgene was turned off, protein aggregates disappeared and neuropathology and behavioral phenotypes reversed.[41] Although the composition of HD- and LGMD1A-associated protein aggregates differ, these data support that aggregates in general are not static and can be targets for therapy. These results in HD mice provide hope that a similar reversal can be achieved in LGMD1A animals with optimization of our MYOT gene silencing strategy.

In conclusion, we showed that RNAi-mediated inhibition of mutant MYOT significantly improved histological and functional outcome measures in a mouse model of LGMD1A. This study was important as an initial proof-of-principle demonstration and justifies further development and optimization of this promising strategy as a potential future treatment for the human disorder.

Materials and methods

Cloning of MYOT-targeted microRNAs. Four different U6 promoter-driven artificial microRNAs targeting human *MYOT* (called miMYOTs) were designed and cloned using strategies previously described by our laboratory.[42] Specifically, the U6.miMYOT constructs were derived from human mir-30 stem and loop sequences with replacement of the 22 nucleotide mature mir-30 duplex by sequences targeting the human *MYOT* gene (**Supplementary Figure S1**). Three criteria were used to select the best candidate miRNAs for initial *in vitro* efficacy testing. First, to assist with proper loading of the antisense guide strand into RNA-induced silencing complex, miRNAs were designed such that the 5′-end of the guide was composed of 3–4 GC bases, while the 3′ end of the molecule contained 3–4 AU bases. Second, the maximum GC content of the guide strand was limited to 60%. Third, sequences with stretches of 4–5 T's were avoided to prevent premature termination of the miRNA transcript, which arose from the pol-III-dependent U6 promoter. Following initial efficacy screening *in vitro*, our lead U6.miMYOT and control miRNAs were then subcloned into AAV.CMV.hrGFP or AAV.CMV.eGFP proviral plasmid upstream of the reporter gene cassette (**Figures 2** and **3**).

Real-time PCR and western blot analysis. For *in vitro* studies, AAV-U6.miMYOT or control microRNA plasmids were transfected into HEK293 cells. RNA or protein was extracted (Trizol from Fisher, Waltham, MA and M-PER from Pierce, Rockford, IL respectively) 48-hour post-transfection. For *in vivo* analysis, RNA or protein was extracted from muscles 3 and 9 months postinjection. Total RNA was DNase-treated (DNA-Free, Ambion by Life Technologies, Carlsbad, CA), and cDNA was synthesized with High Capacity cDNA Reverse Transcription Kit (Applied Biosystems, Foster City, CA). Human *MYOT* transcript was analyzed by real-time RT-PCR using mouse GAPDH as a control (predesigned primer/probe sets, Applied Biosystems). For western blotting, protein was quantified by Lowry assay (BioRad, Hercules, CA), and 10 µg samples were separated on 10% sodium dodecyl sulfate–polyacrylamide gel electrophoresis and transferred to polyvinylidene difluoride membrane. Membranes were incubated with primary antibody overnight at 4 °C. Following washes, blots were then probed with secondary antibody for 1 hour at room temperature and then developed using Immobilon Western horseradish peroxidase substrate (Millipore, Billerica, MA). Primary antibodies for western blot include: mouse monoclonal antibodies to myc-tag (1:5,000; Invitrogen, Grand Island, NY); mouse monoclonal GAPDH antibodies (1:500; Millipore); rabbit polyclonal myotilin antibodies (1:4,000; Bethyl Laboratories, Montgomery, TX).

Animals. Mice hemizygous for human myotilin TgT57I transgene were purchased from Jackson Laboratory (Bar Harbor, ME) and maintained by breeding onto the C57BL/6 background. Male TgT57I and wild-type C57BL/6 littermates were identified by PCR genotyping of genomic DNA from newborn mice (P1) using primers detecting the human MYOT transgene (forward, 5′- GCAAAGATTTTCTGCCTCCTCAAC -3′ and reverse, 5′- GCGGAAGGGATTTTACTGCTATTG -3′) and the mouse Y chromosome (*SRY* gene; forward, 5′-GTGTCACAGAGGAGTGGCATTTTAC-3′ and reverse,

5′-TTGCTGCTGGTGGTGGTTATGG-3′). Male P1 or P2 mice were then injected in the lower limbs with 5×10^{10} DNAse resistant particles per leg with indicated vectors. Muscles were harvested for analysis at 3 and 9 months of age. All mouse protocols were approved by the Institutional Animal Care and Use Committee at The Research Institute of Nationwide Children's Hospital.

Imaging and histology. In vivo AAV transduction was determined by GFP epifluorescence using a fluorescent dissecting microscope (MZ16FA; Leica, Wetzlar, Germany). Dissected muscles were placed in O.C.T. Compound (Tissue-Tek, Torrance, CA) and frozen on liquid nitrogen-cooled 2-methylbutane. The blocks were cut onto slides as 10 µm cryosections, and stained with hematoxylin and eosin (H&E; following standard protocols), or anti-MYOT polyclonal antibodies. For MYOT immunohistochemistry, cryosections were fixed in methanol and blocked in phosphate-buffered saline containing 5% normal goat serum, 0.1% pig gelatin, 1% BSA, and 0.2% Triton X-100. Slides were incubated overnight at 4 °C with MYOT primary antibody (1:400), and then with Alexa-Fluor-594 conjugated goat anti-rabbit secondary antibodies (1:500; 1 hour at room temperature; Molecular Probes, Carlsbad, CA). Images were taken from mouse tissue harvested from 3- and 9-month-old male mice. Muscle cross-sectional fiber diameters and percentage of myofibers with centrally located nuclei were determined from five different animals per group (five fields per leg).

Contractile measurements of gastrocnemius muscle. Mice were anesthetized with intraperitoneal injection of Avertin (250 mg/kg) with supplemental injections given to maintain an adequate level of anesthesia during the whole procedure. The gastrocnemius muscle was exposed and the distal tendon was isolated and cut. The exposed muscle and tendon were kept moist by periodic applications of isotonic saline. A knot was tied at the proximal end of the tendon and the mouse was placed on a heated platform maintained at 37 °C. The tendon was tied securely to the lever arm of a servomotor (6650LR; Cambridge Technology, Bedford, MA) via the suture ends. The muscle was then stimulated with 0.2 ms pulses via the tibial nerve using platinum electrodes. Stimulation voltage and muscle length (L_o) were adjusted for maximum isometric twitch force (P_t). While held at L_o, the muscle was stimulated at increasing frequencies until maximum force (P_o) was reached. Optimum fiber length (L_f) was determined by multiplying L_o by a previously determined L_f/L_o ratio of 0.45. Total fiber cross-sectional area was calculated by dividing the muscle mass (mg) by the product of L_f (mm) and the density of mammalian skeletal muscle, 1.06 g/cm^2. Specific P_o (N/cm^2) was calculated by dividing P_o by total fiber cross-sectional area for each muscle. Immediately after muscle mass was measured, muscles were coated in tissue freezing medium (Triangle Biomedical Sciences, Durham, NC), frozen in isopentane cooled by dry ice, and stored at –80 °C until needed.

Extensor digitorum longus muscle contractile measurements. The extensor digitorum longus muscle was isolated from the hind limbs of the mice. A 5–0 silk suture was tied to the proximal and distal tendons of the muscle, and the tendons were cut. The muscle was removed and immediately placed in a bath containing Krebs' mammalian Ringer solution with 0.25 mmol/l tubocurarine chloride. The solution was maintained at 25 °C and bubbled with 95% O_2 and 5% CO_2. The distal tendon was attached to a servomotor (model 305B; Aurora Scientific, Aurora, ON). The proximal tendon was attached to a force transducer (model BG-50; Kulite Semiconductor Products, Leonia, NJ). The muscle was stimulated by square-wave pulses delivered by two platinum electrodes connected to a high-power biphasic current stimulator (model 701B; Aurora Scientific). The voltage of pulses was increased, and L_o was determined as described above. Muscles were held at L_o, and stimulus frequency was increased until the P_o was achieved. An L_f/L_o ratio of 0.44 for extensor digitorum longus muscles was used to calculate L_f. Total fiber cross-sectional area was determined by dividing the mass of the muscle by the product of L_f and 1.06 g/cm^3, the density of mammalian skeletal muscle-specific P_o was determined by dividing P_o by the total fiber cross-sectional area.

Statistical analysis. All data are expressed as mean ± SEM. Statistical analyses were performed using the GraphPad Prizm software package (GraphPad Software, La Jolla, CA). Statistical tests used for each experiment, and accompanying N's, are indicated in the figure legends.

Supplementary material

Figure S1. Sequence and binding position of miMYOTs.
Figure S2. Typical transduction achieved in the GAS muscles following 5×10^{10} particles of AAV.miMYOT or AAV.control vectors carrying CMV.hrGFP (left) or CMV.eGFP (right) reporters.
Figure S3. Representative cryosection from a WT mouse treated with 5×10^{10} particles of AAV.miMYOT vector, 3 months postinjection.
Figure S4. The 3 month timepoint is not optimal for muscle physiology outcome measures in TgT57I mice.
Figure S5. Preliminary toxicology report supporting the safety of AAV.miMYOT vectors.

Acknowledgments. This work was supported by an NINDS Translational R21 grant (1R21NS072260-01, to S.Q.H). For 1 year during the course of this study, L.M.W. was postdoctoral fellow on NIH training grant T32 NS077984. We thank Louise Rodino-Klapac for technical assistance. D.D.S. was supported by NIA training grant AG-000114.

1. Hauser, MA, Conde, CB, Kowaljow, V, Zeppa, G, Taratuto, AL, Torian, UM *et al.* (2002). myotilin Mutation found in second pedigree with LGMD1A. *Am J Hum Genet* **71**: 1428–1432.
2. Hauser, MA, Horrigan, SK, Salmikangas, P, Torian, UM, Viles, KD, Dancel, R *et al.* (2000). Myotilin is mutated in limb girdle muscular dystrophy 1A. *Hum Mol Genet* **9**: 2141–2147.
3. Gilchrist, JM, Pericak-Vance, M, Silverman, L and Roses, AD (1988). Clinical and genetic investigation in autosomal dominant limb-girdle muscular dystrophy. *Neurology* **38**: 5–9.
4. Olivé, M, Goldfarb, LG, Shatunov, A, Fischer, D and Ferrer, I (2005). Myotilinopathy: refining the clinical and myopathological phenotype. *Brain* **128**(Pt 10): 2315–2326.
5. Pénisson-Besnier, I, Talvinen, K, Dumez, C, Vihola, A, Dubas, F, Fardeau, M *et al.* (2006). Myotilinopathy in a family with late onset myopathy. *Neuromuscul Disord* **16**: 427–431.
6. Reilich, P, Krause, S, Schramm, N, Klutzny, U, Bulst, S, Zehetmayer, B *et al.* (2011). A novel mutation in the myotilin gene (MYOT) causes a severe form of limb girdle muscular dystrophy 1A (LGMD1A). *J Neurol* **258**: 1437–1444.

7. Selcen, D and Engel, AG (2004). Mutations in myotilin cause myofibrillar myopathy. *Neurology* **62**: 1363–1371.
8. Selcen, D, Ohno, K and Engel, AG (2004). Myofibrillar myopathy: clinical, morphological and genetic studies in 63 patients. *Brain* **127**(Pt 2): 439–451.
9. Vattemi, G, Neri, M, Piffer, S, Vicart, P, Gualandi, F, Marini, M *et al.* (2011). Clinical, morphological and genetic studies in a cohort of 21 patients with myofibrillar myopathy. *Acta Myol* **30**: 121–126.
10. Schröder, R and Schoser, B (2009). Myofibrillar myopathies: a clinical and myopathological guide. *Brain Pathol* **19**: 483–492.
11. Godley, LA, Lai, F, Liu, J, Zhao, N and Le Beau, MM (1999). TTID: A novel gene at 5q31 encoding a protein with titin-like features. *Genomics* **60**: 226–233.
12. Mologni, L, Moza, M, Lalowski, MM and Carpén, O (2005). Characterization of mouse myotilin and its promoter. *Biochem Biophys Res Commun* **329**: 1001–1009.
13. Keduka, E, Hayashi, YK, Shalaby, S, Mitsuhashi, H, Noguchi, S, Nonaka, I *et al.* (2012). *In vivo* characterization of mutant myotilins. *Am J Pathol* **180**: 1570–1580.
14. Salmikangas, P, van der Ven, PF, Lalowski, M, Taivainen, A, Zhao, F, Suila, H *et al.* (2003). Myotilin, the limb-girdle muscular dystrophy 1A (LGMD1A) protein, cross-links actin filaments and controls sarcomere assembly. *Hum Mol Genet* **12**: 189–203.
15. Schröder, R, Reimann, J, Salmikangas, P, Clemen, CS, Hayashi, YK, Nonaka, I *et al.* (2003). Beyond LGMD1A: myotilin is a component of central core lesions and nemaline rods. *Neuromuscul Disord* **13**: 451–455.
16. Shalaby, S, Mitsuhashi, H, Matsuda, C, Minami, N, Noguchi, S, Nonaka, I *et al.* (2009). Defective myotilin homodimerization caused by a novel mutation in MYOT exon 9 in the first Japanese limb girdle muscular dystrophy 1A patient. *J Neuropathol Exp Neurol* **68**: 701–707.
17. von Nandelstadh, P, Soliymani, R, Baumann, M and Carpen, O (2011). Analysis of myotilin turnover provides mechanistic insight into the role of myotilinopathy-causing mutations. *Biochem J* **436**: 113–121.
18. Garvey, SM, Miller, SE, Claflin, DR, Faulkner, JA and Hauser, MA (2006). Transgenic mice expressing the myotilin T57I mutation unite the pathology associated with LGMD1A and MFM. *Hum Mol Genet* **15**: 2348–2362.
19. Fire, A, Xu, S, Montgomery, MK, Kostas, SA, Driver, SE and Mello, CC (1998). Potent and specific genetic interference by double-stranded RNA in Caenorhabditis elegans. *Nature* **391**: 806–811.
20. Liu, J and Harper, SQ (2012). RNAi-based gene therapy for dominant Limb Girdle Muscular Dystrophies. *Curr Gene Ther* **12**: 307–314.
21 Wallace, LM, Garwick, SE and Harper, SQ. Rnai therapy for dominant muscular dystrophies and other myopathies. In: Duan D (ed.). *Muscle Gene Therapy*. Springer: New York, 2010, 99–115.
22. Wallace, LM, Garwick-Coppens, SE, Tupler, R and Harper, SQ (2011). RNA interference improves myopathic phenotypes in mice over-expressing FSHD region gene 1 (FRG1). *Mol Ther* **19**: 2048–2054.
23. Wallace, LM, Liu, J, Domire, JS, Garwick-Coppens, SE, Guckes, SM, Mendell, JR *et al.* (2012). RNA interference inhibits DUX4-induced muscle toxicity in vivo: implications for a targeted FSHD therapy. *Mol Ther* **20**: 1417–1423.
24. McBride, JL, Boudreau, RL, Harper, SQ, Staber, PD, Monteys, AM, Martins, I *et al.* (2008). Artificial miRNAs mitigate shRNA-mediated toxicity in the brain: implications for the therapeutic development of RNAi. *Proc Natl Acad Sci USA* **105**: 5868–5873.
25. High, KA (2011). Gene therapy for haemophilia: a long and winding road. *J Thromb Haemost* **9** (suppl. 1): 2–11.
26. Mendell, JR, Rodino-Klapac, LR, Rosales, XQ, Coley, BD, Galloway, G, Lewis, S *et al.* (2010). Sustained alpha-sarcoglycan gene expression after gene transfer in limb-girdle muscular dystrophy, type 2D. *Ann Neurol* **68**: 629–638.
27. Mendell, JR, Rodino-Klapac, LR, Rosales-Quintero, X, Kota, J, Coley, BD, Galloway, G *et al.* (2009). Limb-girdle muscular dystrophy type 2D gene therapy restores alpha-sarcoglycan and associated proteins. *Ann Neurol* **66**: 290–297.
28. Blankinship, MJ, Gregorevic, P, Allen, JM, Harper, SQ, Harper, H, Halbert, CL *et al.* (2004). Efficient transduction of skeletal muscle using vectors based on adeno-associated virus serotype 6. *Mol Ther* **10**: 671–678.
29. Garwick-Coppens, SE, Herman, A and Harper, SQ (2011). Construction of permanently inducible miRNA-based expression vectors using site-specific recombinases. *BMC Biotechnol* **11**: 107.
30. Harper, SQ, Hauser, MA, DelloRusso, C, Duan, D, Crawford, RW, Phelps, SF *et al.* (2002). Modular flexibility of dystrophin: implications for gene therapy of Duchenne muscular dystrophy. *Nat Med* **8**: 253–261.
31. Fischer, D, Kley, RA, Strach, K, Meyer, C, Sommer, T, Eger, K *et al.* (2008). Distinct muscle imaging patterns in myofibrillar myopathies. *Neurology* **71**: 758–765.
32. McNeill, A, Birchall, D, Straub, V, Goldfarb, L, Reilich, P, Walter, MC *et al.* (2009). Lower limb radiology of distal myopathy due to the S60F myotilin mutation. *Eur Neurol* **62**: 161–166.
33. Mologni, L, Salmikangas, P, Fougerousse, F, Beckmann, JS and Carpén, O (2001). Developmental expression of myotilin, a gene mutated in limb-girdle muscular dystrophy type 1A. *Mech Dev* **103**: 121–125.
34. Wallace, LM, Moreo, A, Clark, KR and Harper, SQ (2013). Dose-dependent Toxicity of Humanized Renilla reniformis GFP (hrGFP) Limits Its Utility as a Reporter Gene in Mouse Muscle. *Mol Ther Nucleic Acids* **2**: e86.
35. McCarty, DM (2008). Self-complementary AAV vectors; advances and applications. *Mol Ther* **16**: 1648–1656.
36. Gregorevic, P, Blankinship, MJ, Allen, JM, Crawford, RW, Meuse, L, Miller, DG *et al.* (2004). Systemic delivery of genes to striated muscles using adeno-associated viral vectors. *Nat Med* **10**: 828–834.
37. Rodino-Klapac, LR, Montgomery, CL, Mendell, JR and Chicoine, LG (2011). AAV-mediated gene therapy to the isolated limb in rhesus macaques. *Methods Mol Biol* **709**: 287–298.
38. Mendell, JR, Rodino-Klapac, L, Sahenk, Z, Malik, V, Kaspar, BK, Walker, CM *et al.* (2012). Gene therapy for muscular dystrophy: lessons learned and path forward. *Neurosci Lett* **527**: 90–99.
39. Moza, M, Mologni, L, Trokovic, R, Faulkner, G, Partanen, J and Carpén, O (2007). Targeted deletion of the muscular dystrophy gene myotilin does not perturb muscle structure or function in mice. *Mol Cell Biol* **27**: 244–252.
40. Rodriguez-Lebron, E and Paulson, HL (2006). Allele-specific RNA interference for neurological disease. *Gene Ther* **13**: 576–581.
41. Yamamoto, A, Lucas, JJ and Hen, R (2000). Reversal of neuropathology and motor dysfunction in a conditional model of Huntington's disease. *Cell* **101**: 57–66.
42 Boudreau, RL, Garwick-Coppens, SE, Liu, J, Wallace, LM and Harper, SQ. Rapid cloning and validation of Microrna shuttle vectors: a practical guide. In: Harper, SQ (ed.). *Rna Interference Techniques*. Humana Press: New York, 2011, 19–37.

Supplementary Information accompanies this paper on the Molecular Therapy–Nucleic Acids website (http://www.nature.com/mtna)